Comparisons of cloud top heights derived from lidar and radar observations and levels of neutral buoyancy

Seiji Kato[a], David P. Duda[b], Kuan-Man Xu[a], Seung-Hee Ham[a], Sunny Sun-Mack[b], Yan Chen[b], and Walter F. Miller[c]

a NASA Langley Research Center, Hampton, Virginia.
b Analytical Mechanics Associates (AMA), Inc, Hampton, Virginia
c ADNET Systems, Inc. Reston, Virginia

1. Introduction

The structure of convective clouds and processes within them are complex. A simplified view of a convective cloud is based upon parcel theory, which assumes that a parcel of air originating in the boundary layer is lifted adiabatically to the level of neutral buoyancy (LNB). How actual convective cloud and anvil cloud top heights are different from the level of neutral buoyancy has an important implication to radiation budget because their cloud top temperature determines outgoing longwave radiation.

Unlike cloud top heights derived from passive sensors, cloud top heights derived from Cloud-Aerosol Lidar and Infrared Pathfinder Satellite Observations (CALIPSO, Winker et al. 2009) and CloudSat (Stephens et al. 2008) observations are derived directly from their signals, independently from temperature profiles. Therefore, CALIPSO/CloudSat cloud top heights are independent from errors in temperature, hence more accurate than those derived from passive sensors. In this study, we compare cloud top heights derived from the active sensors and LNB

2. Data product and method

We use deep convective cloud objects derived from Moderate Resolution Imaging Spectroradiometer (MODIS) observations collocated with Clouds and the Earth's Radiant Energy System (CERES) and CALIPSO and CloudSat observations. Deep convective cloud objects are derived from Aqua MODIS for regions between 25ºS and 25ºN using daytime observation (Xu et al. 2005, 2016). Selection criteria for deep convective cloud objects are 1) cloud top height higher than 10 km, 2) cloud optical thickness greater than 10, and 3) overcast over a CERES footprint (approximately a 20 km diameter at nadir). We use MERRA-2 temperature and humidity profiles collocated with cloud objects. Cloud top heights are derived from CALIPSO and CloudSat by the method described in Kato et al (2010).

3. Results

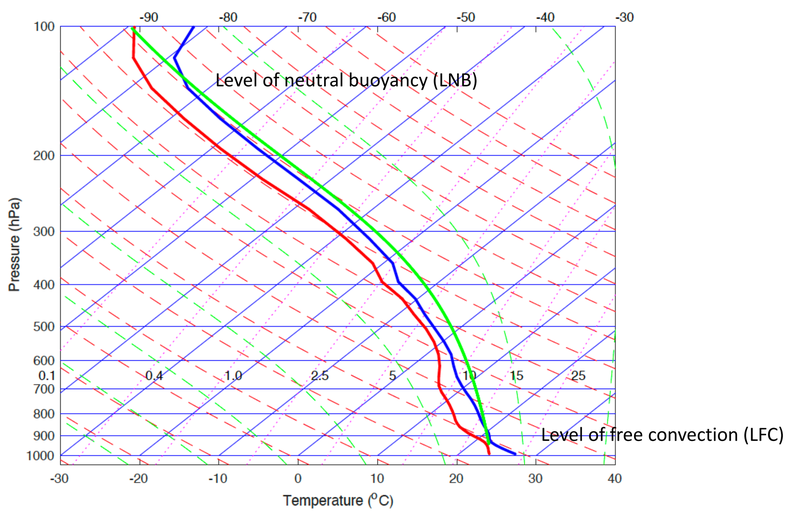

Figure 1: Skew-t diagram of MERRA-2 temperature (blue) and dew point (red) profiles. The profiles fall within a deep convective cloud object are averaged. A parcel lifted from surface raises adiabatically to the lifting condensation level (LCL). Green line is moist adiabat computed from LCL to the level of neutral buoyancy (LNB). Convective available potential energy (CAPE) is computed integrating the difference of virtual temperature of the parcel and virtual temperature of environment multiplied by the dry air gas constant from the level of free convection (LFC) to LNB, which is approximately the area between the blue and green lines.

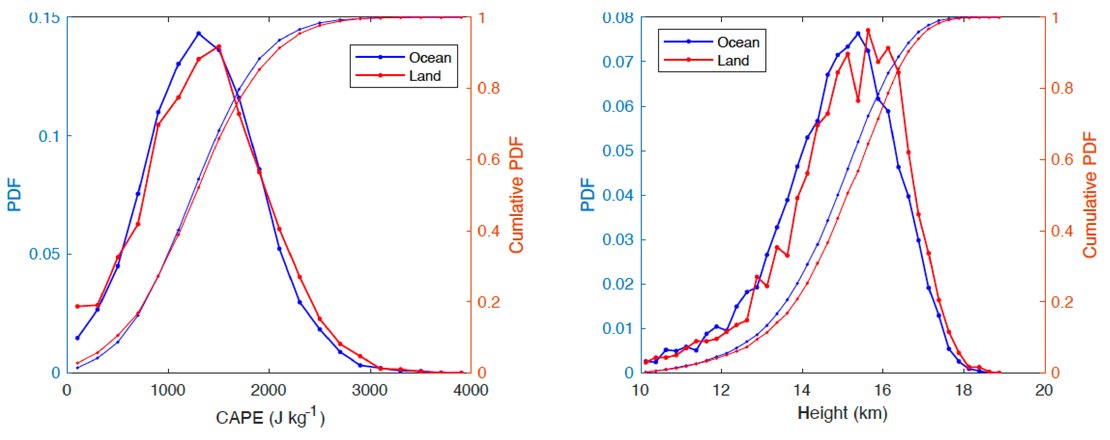

Figure 2: Normalized frequency of occurrence of (left) convective available potential energy (CAPE) and (right) cloud top height derived from CALIPSO and CloudSat observations for deep convective cloud objects. Blue and red lines are for deep convective clouds present over ocean and land, respectively. The mean difference (standard deviation) of cloud top height minus LNB is 0.46 km (1.17 km) over ocean and 0.68 km (1.32 km) over land. When both ocean and land deep convective clouds are combined, 12% of the cloud top heights is within ±0.2 km from the LNB. The width of bins is 200 J kg^{-1} for CAPE and 0.25 km for height. Blue and red thin lines are cumulative distribution for ocean and land, respectively.

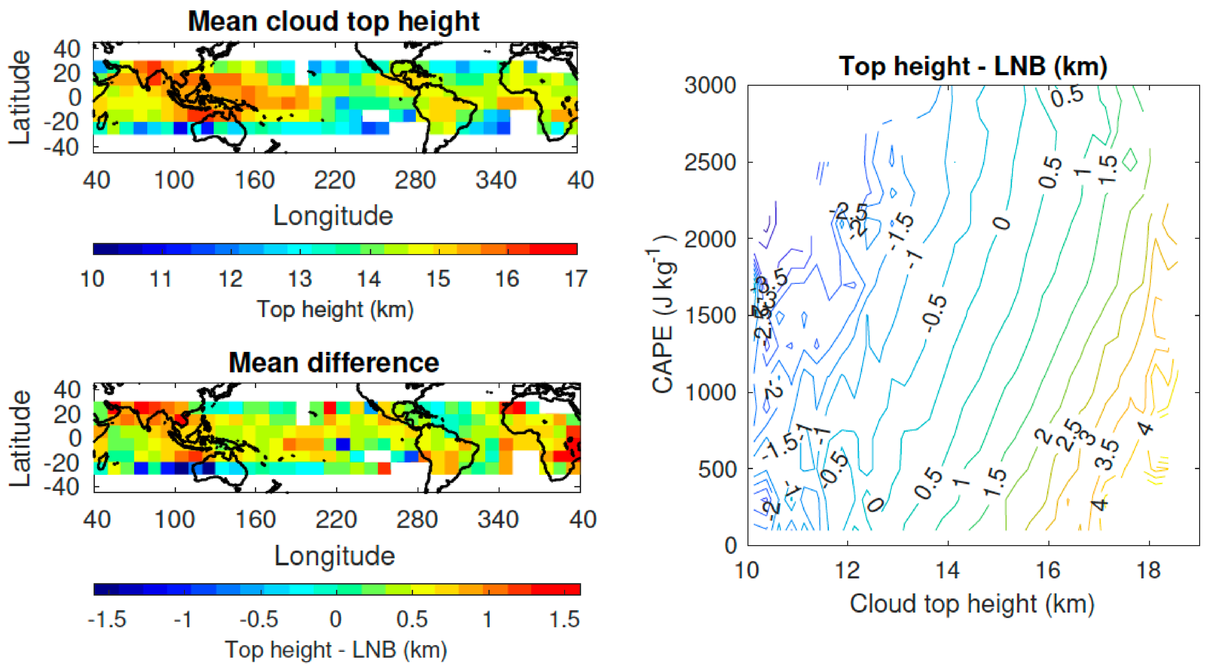

Figure 3: (Top left) Mean cloud top height of deep convective clouds and (bottom left) mean difference between cloud top height and level of neutral buoyancy. (Right) Difference between the level of neutral buoyancy and cloud top height derived from CALIPSO and CloudSat as a function of cloud top height and CAPE.

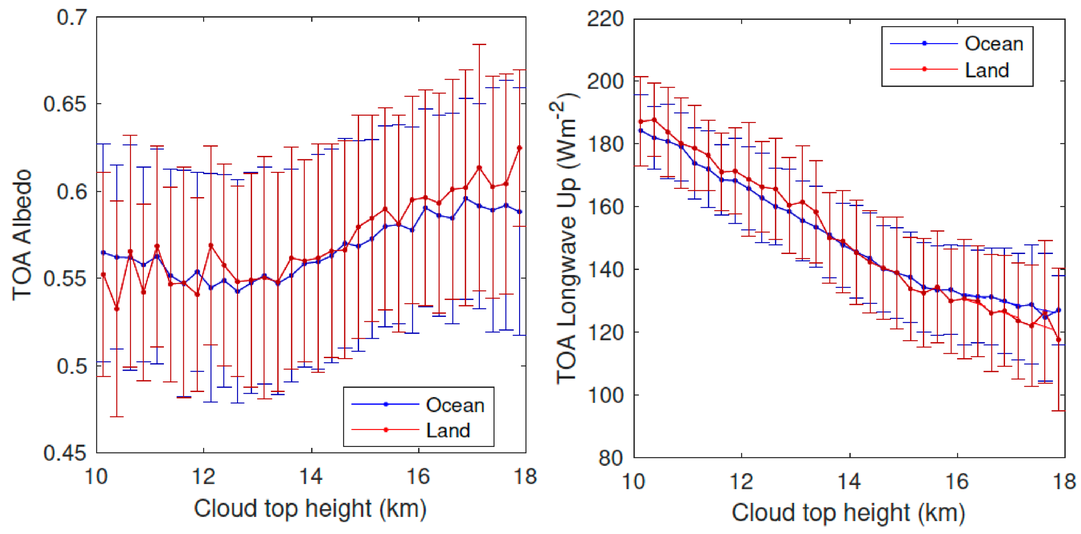

Figure 4: Top) Top-of-atmosphere albedo (left) and upward longwave irradiance (right) derived from CERES observations for ocean (blue line) and land (red line) deep convective cloud objects. Error bars indicate maximum and minimum values for the time period from July 2006 through June 2010. The rate of decreasing upward longwave irradiance is 7.7±4.6 Wm^{-2} km^{-1} for ocean and 9.1±1.2 Wm^{-2} km^{-1} for land. The rate of decreasing upward longwave irradiance when cloud top height is below 16 km is 9.4±0.4 Wm^{-2} km^{-1} for ocean and 10.5±0.6 Wm^{-2} km^{-1} for land and cloud top height above 16 km is 4.2±0.7 Wm-2 km^{-1} for ocean and 8.7±5.7 Wm^{-2} km^{-1} for land.

4. Summary

Cloud top heights of deep convective clouds derived from lidar and radar observations are analyzed as a function of convective available potential energy (CAPE) and compared with the level of neutral buoyancy (LNB). The mean difference (standard deviation) of cloud top height minus LNB is 0.46 km (1.17 km) over ocean and 0.68 km (1.32 km) over land. The mean difference of cloud top height of 0.46 km and 0.68 km correspond to a bias of upward longwave irradiance of 3.5 Wm^{-2} for ocean and 6.2 Wm^{-2} for land.

References and Acknowledgements

Kato, S., S. Sun-Mack, W. F. Miller, F. G. Rose, Y. Chen, P. Minnis, and B. A. Wielicki, 2010: Relationships among cloud occurrence frequency, overlap, and effective thickness derived from CALIPSO and CloudSat merged cloud vertical profiles, *J. Geophys. Res*. 115 D00H28, doi:10.1029/2009JD012277.

Stephens, G. L., and coauthors, 2009: CloudSat mission: Performance and early science after the first year of operation, *J. Geophys. Res*., 113, D00A18, DOI:10.1029/2008JD009982.

Winker, D. M., M. A. Vaughan, A. Omar, Y,-X. Hu, K. A. Powell, Z. Liu, W. H. Hunt, and S. A. Young, 2009: Overview of the CALIPSO mission and CALIOP data processing algorithms, *J. Atms. Ocean. Technol*., 26, 2310-2323, doi: 10.1175/2009JTECHA1281.1.

Xu, K.-M., T. Wong, S. Dong, F. Chen, S. Kato, and P. C. Taylor, 2016: Clou objects analysis of CERES Aqua observations of tropical and subtropical cloud regimes: Four-year climatology, *J. Climate*, 29, 1617-1638, DOI: 10.1175/JCLI-D-14-00836.1.